JOURNAL OF SPACECRAFT AND ROCKETS
Vol. 43, No. 5, September–October 2006

Numerical Study of Behavior of Outgas from Heat Shield of Solar Probe

Kojiro Suzuki*
University of Tokyo, Chiba 277-8561, Japan

When a solar probe penetrates into the solar corona for in-situ observation of the solar wind, the graphitic heat shield temperature is expected to increase to over 2000 K and surface sublimation will occur. The sublimation gas is numerically studied by using the direct simulation Monte Carlo method. The length scale and the Knudsen number are evaluated with respect to the interaction phenomena between the solar wind and the outgas from the heat shield. When the total sublimation rate and the number density of the solar wind are large, the velocity distribution function of the solar wind around the probe is expected to become quite different from that of the undisturbed freestream due to molecular collisions. Numerical results indicate that the total sublimation rate must be 10^{-6} kg/s or lower to avoid serious errors in the solar wind measurements. Thermal analyses show that the inclined graphitic disk heat shield can satisfy this requirement. Detailed rarefied flow simulation is also made around the spacecraft consisting of the heat shield and the main body. Favorable location for the sensor is discussed from a viewpoint of the solar wind observation.

Nomenclature

c_{av}	=	average molecular speed
c_{mp}	=	most probable molecular speed
d	=	molecular diameter
J	=	mass flux per unit time and unit area
Kn	=	Knudsen number
L	=	length scale for interaction between solar wind and sublimation gas cloud
M	=	molecular weight
m_p	=	particle mass
n	=	number density
p_{eva}	=	equilibrium vapor pressure
q	=	solar radiative heating per unit area
R	=	universal gas constant
Rs	=	solar radius
S	=	area of heat shield
T	=	temperature
x	=	distance between solar probe and heliocenter
λ	=	mean free path

Subscripts

i	=	ith species
sub	=	sublimation gas
w	=	condition at wall
∞	=	freestream condition of solar wind

I. Introduction

THE mechanism of the acceleration and heating of the solar wind in the corona is one of the most important unsolved problems in space science. Close-approach in situ observations are expected to give us a key to solve the problem. Though the solar probe mission has been studied for more than two decades,[1–7] technical and financial difficulties have prevented its realization. However, recent technological advancements in the trajectory design, down-sizing of the spacecraft instruments, thermal protection, and so on, enable one to plan a low-cost small solar probe mission.[4,5]

One of the most critical problems of the solar probe is the design of the heat shield to protect the instruments of the spacecraft from severe heating of the solar radiation at close approach to the sun. When its scientific objectives are considered, the probe must penetrate into the solar corona and the minimum distance from the heliocenter is expected to be 3–5 solar radii Rs. In the case of $4Rs$, the heat flux of the solar radiation will become about 4 MW/m^2, which is in the same order as the aerodynamic heating of Earth's re-entry. At present, a heat shield fabricated from carbon–carbon (C/C) or graphitic material seems promising from the viewpoints of thermal resistibility and low mass density.[4] During the solar flyby, however, the heat shield temperature is expected to increase to over 2000 K and outgassing from the heat shield will occur due to surface sublimation. When the sublimation rate is high, a thick cloud of the sublimation gas will be formed around the spacecraft. It will significantly interact with the solar wind through molecular collisions. For this situation, the properties of the solar wind detected by the sensors on the probe are expected to be quite different from those of the undisturbed freestream, becoming a major problem for the solar probe mission. Consequently, the effect of the outgassing on the coronal environment must be evaluated in the design of the solar probe. In the previous studies of solar probe design, it has been pointed out that the total sublimation rate from the heat shield must be limited to limit interference with science instruments.[4,5] However, the main concern was in the measurement error due to the presence of the sublimation gas in the vicinity of the scientific sensors. The behavior of the outgas from the heat shield in the solar wind has not been well understood. The effects of the sublimation gas should be qualitatively and quantitatively investigated by rarefied gasdynamics analyses from the viewpoints of 1) the interaction between the solar wind and the sublimation gas and 2) their behavior around the spacecraft.

In the present study, the rarefied flows of the sublimation gas and the solar wind are numerically studied with the direct simulation Monte Carlo (DSMC) method, because the number density of the solar wind is quite low even in the corona. The research objectives are as follows: 1) to identify a favorable configuration for the solar probe heat shield from the viewpoint of reducing the sublimation rate; 2) to clarify the feature of the rarefied flow environment around the solar probe; 3) to investigate how the solar wind properties are affected by the interaction with the sublimation gas cloud around the probe, and to determine the maximum allowable sublimation

Presented as Paper 2004-2271 at the AIAA 37th Thermophysics Conference, Portland, OR, 28 June–1 July 2004; received 17 August 2005; revision received 17 November 2005; accepted for publication 29 November 2005.

*Associate Professor, Department of Advanced Energy, Graduate School of Frontier Sciences, 5-1-5 Kashiwa-no-ha. Senior Member AIAA.

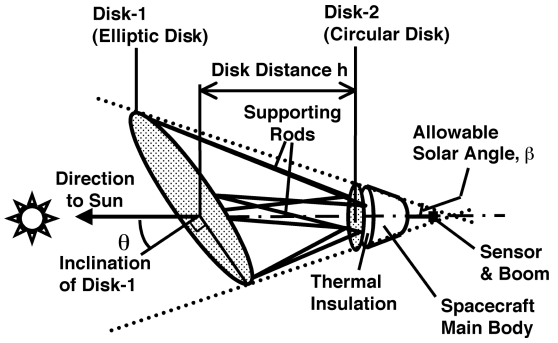

Fig. 1 Design concept of heat shield with elliptic and circular disks.

rate from the viewpoint of the solar wind observation; and 4) to obtain the detailed flow structure around the spacecraft configuration, and to identify the location of sensors suitable for the solar wind observation.

II. Shape of Heat Shield for Solar Probe Mission

For the solar probe, two types of heat shield configuration have been proposed, that is, the conical type[1,3,6,7] and the dish type.[4,5] In the present study, we consider the heat shield consisting of two disks as shown in Fig. 1. Note that this is an outdated design and that the conical geometry is currently considered for the solar probe.[7] The primary shield (disk 1 in Fig. 1) is an elliptic disk inclined at angle θ to the solar direction. It is set in front of the secondary shield (disk 2) at distance h measured along the centerline of disk 2. The secondary shield is a circular disk with radius r_2. Behind disk 2, the main body of the spacecraft is located. For simplicity of analysis, these disks are assumed to be flat. We set the allowable solar angle β considering the viewing angle of the edge of the photosphere from the spacecraft at the closest approach to the sun. In the present study, we assume that r_2 and the length of the main body are 0.5 and 1 m, respectively, after the studies in Refs. 4 and 5. The angle β is set as 15 deg, assuming that the distance between the probe and the heliocenter is $4Rs$ at the closest approach. Once the values of θ and h are given, the configuration of disk 1 is automatically determined so that the whole body is in the umbra of half-angle β. On the backside of disk 2, no heat transfer and no sublimation are assumed.

The radiative heating per unit area from the sun is predicted by the relation[3]

$$q = q_0(Rs/x)^2, \qquad q_0 = 6.24 \times 10^7 \text{ W/m}^2 \tag{1}$$

where Rs and x are the solar radius and the distance from the heliocenter to the probe, respectively. When it is assumed that the temperature is uniform on each disk due to high thermal conductivity of the graphitic material, the shield temperature is predicted by considering the energy balance of the incoming solar flux, the radiative cooling, and the radiative heat transfer between two disks. The radiative heat transfer is calculated by using the configuration factor,[8] which represents the ratio of the radiative flux reaching one disk to the total heat flux radiated from the other disk. The configuration factor is calculated by numerical integration considering the geometric relation between these disks. The ratio of the solar absorptance to emittance is set as unity, which is a good approximation for the graphitic material at around 2300 K (Ref. 9). The latent heat of sublimation is ignored because it is much smaller than the solar radiation and the reduction in the heat shield temperature by the latent heat is smaller than 1%, even when the probe is located at 2.5 Rs and the sublimation rate is much larger than the nominal case.

When the temperature of the graphitic material becomes high at close approach to the sun, sublimation occurs and the gases of C, C_2, C_3, and so, on are injected at the surface to the ambient. The sublimation rate is estimated from the wall temperature T_w by the

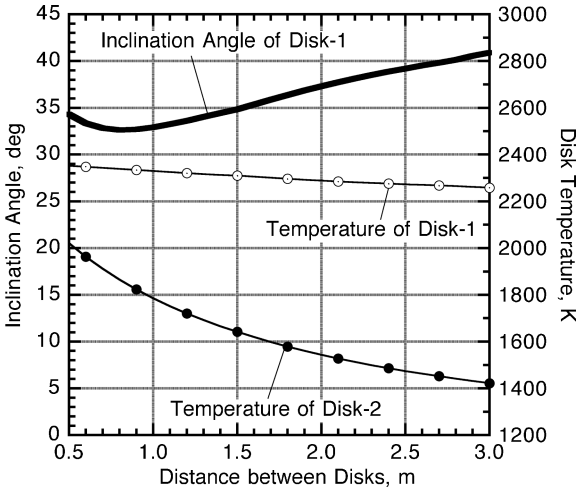

Fig. 2 Effects of disk distance on inclination angle and temperature of heat shield.

Hertz–Knudsen–Langmuir relation,[10]

$$J_{\text{sub}} = \sum_i \frac{\alpha_i \, p_{\text{eva},i}}{\sqrt{2\pi(R/M_i)\,T_w}}, \qquad i = C, C_2, C_3, \ldots \tag{2}$$

where α, M, and p_{eva} are the sublimation efficiency, molecular weight of the sublimation gas, and the equilibrium vapor pressure, respectively. In the present study, the sublimation parameters in Ref. 10 are used. The dominant species of the sublimation gas is monatomic carbon for temperature lower than about 2500 K. The effect of the ambient pressure on the sublimation rate is ignored because the wall pressure induced by the molecular collision in the vicinity of the surface is much smaller than the equilibrium vapor pressure under the heating environment at the perihelion. In fact, the rarefied flow analyses show that the reduction in the sublimation rate due to the wall pressure is smaller than 3% even when the probe is at $2.5Rs$.

We assume that the minimum distance between the solar probe and the heliocenter is $4Rs$ in the nominal case. Considering the effects of interaction between the solar wind and the sublimation gas cloud, as discussed later, we set the limit for the total sublimation rate as 2×10^{-6} kg/s, which seems consistent with the design constraint (2.5×10^{-6} kg/s) in the study at NASA Jet Propulsion Laboratory (JPL).[4] Figure 2 shows the variation of the minimum inclination angle θ and the temperature of disks 1 and 2 with the distance h for this constraint to be satisfied at $4Rs$. The temperature of disk 1 and the sublimation rate are reduced by inclining disk 1. The total sublimation rate is given as the product of the sublimation rate per unit area and the heat shield area. The latter increases and the former decreases more rapidly with the increase in the angle θ. Hence, the minimum inclination angle is calculated for distance h. When the distance h increases, the temperature of disk 2 decreases because the solid angle of disk 1 viewed from disk 2 becomes small. However, the area of disk 1, the length of supporting rods (Fig. 1), and, consequently, the mass of the heat shield increase. In the present study, we assume the maximum allowable temperature of disk 2 to be 1500 K. To minimize the heat shield mass, the values of θ and h are determined as 38.5 deg and 2.3 m, respectively. In this case, the semimajor and semiminor radii of disk 1 are 1.5 and 1.15 m. The spacecraft shape in Fig. 1 is drawn assuming these values. The flow analyses in the present study are made for this configuration, which is similar to the solar probe considered in the study at JPL.[4]

III. Method of Analysis for Rarefied Flow Around Solar Probe

To investigate the effects of outgassing from the heat shield, the rarefied flow enveloping the solar probe is numerically analyzed. There are two length scales associated with the outgassing. In the near-field analysis with a length scale of the spacecraft size, our

main concern is to clarify the rarefied gas environment in the vicinity of the solar probe, for example, determining the location of the sensors for solar wind observation. On the other hand, the interaction phenomena between the solar wind and the sublimation gas cloud are expected to occur for a length scale larger than the spacecraft size because the velocity of the solar wind is extremely high and the distance between collisions may be quite large. To clarify such phenomena, the far-field analysis with a large length scale is necessary. In the present study, two types of rarefied gas simulations are conducted with two different length scales as discussed in the following sections.

A. Near-Field Analysis

1. Length Scale Consideration

In the near-field analysis, the length scale of the phenomena depends on the behavior of the sublimation gas near the surface of the heat shield. In this section, we only consider a flat graphitic disk set normal to the solar direction. To judge whether the flow of the sublimation gas is free molecular, it is necessary to calculate the smallest mean free path, which is obtained for this condition. The equilibrium temperature is calculated as a function of the distance from the heliocenter, by considering the solar radiation given by Eq. (1) and the radiative cooling from both sides of the heat shield. As the sublimation gas species, only monatomic carbon is considered because the wall temperature is lower than 2500 K in the nominal case and the dominant species of the sublimation gas is monatomic carbon in such temperature region. When it is assumed that the sublimation gas is injected with the Maxwellian velocity distribution at the wall temperature T_w, the number density of the sublimation gas at the surface is predicted by using the mean injection velocity v_w as[11]

$$n_w = (J_{\text{sub}}/m_p)/v_w, \qquad v_w = \sqrt{(R/M_C)T_w/2\pi} \tag{3}$$

where m_p is the mass of the sublimation gas particle and the sublimation rate per unit area J_{sub} is given by Eq. (2). In the present study, the hard sphere model[12] with the constant particle diameter d of 3.4×10^{-10} m is used for monatomic carbon.[13] Then the mean free path is calculated by the relation[14]

$$\lambda = 1\Big/\sqrt{2}\pi\, d^2 n_w \tag{4}$$

The variations of the equilibrium wall temperature and the mean free path with the distance between the probe and the heliocenter are shown in Fig. 3. When the distance from the heliocenter becomes smaller than $3.5Rs$, the mean free path is smaller than 3 m, which is almost the same as a length scale of the spacecraft. In the near-field analysis, the Knudsen number is defined as the ratio of the mean free path to the spacecraft size. Consequently, in the case of close approach at smaller distance than the nominal ($4Rs$), the Knudsen

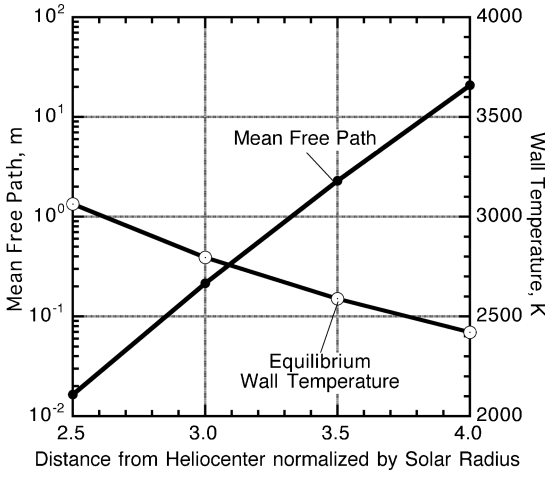

Fig. 3 Variations of equilibrium wall temperature and mean free path with distance from heliocenter.

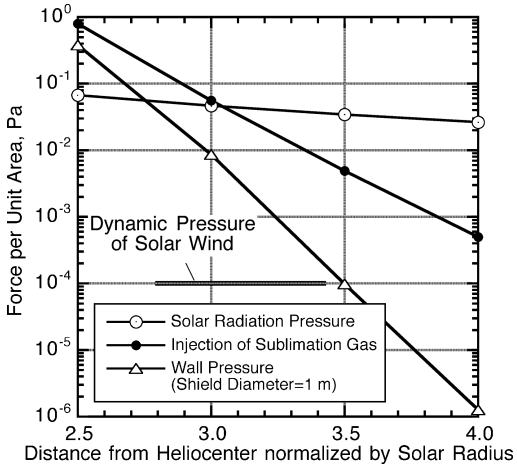

Fig. 4 Comparison of various types of forces acting on heat shield per unit area.

number becomes smaller than unity. In such a case, the flow around the spacecraft cannot be taken as free molecular, and the collision between particles must be considered in the analyses.

When the sublimation gas is not free molecular, the heat shield surface pressure is enhanced due to the molecular collision. The wall pressure is compared with the solar radiation pressure, thrust due to the mass injection of sublimation, and the dynamic pressure of the solar wind in Fig. 4. To calculate the wall pressure, two-dimensional flow of the sublimation gas around a heat shield is analyzed by the DSMC method. As the heat shield, a flat plate of width 1 m is assumed to be set normal to the solar direction. Detail of the analysis is described in Ref. 15. In the present study, we assume that the solar wind is in the same direction as the solar radiation, though the direction of the solar wind does not necessarily coincide with that of the solar radiation due to the effect of the sun's rotation. The oblique impact of the solar wind at the heat shield may occur even when the heat shield is set normal to the solar radiation. The dynamic pressure of the solar wind is so small that the impact pressure is negligible in comparison with the other types of forces. When the distance from the heliocenter is smaller than $3Rs$, the injection thrust becomes the largest force. The wall pressure is smaller than the injection thrust, but it increases more rapidly than the injection thrust with the decrease in the distance from the sun. The wall pressure also depends on the size of the heat shield. Larger wall pressure will be generated for larger heat shield because the Knudsen number decreases and the molecular collision becomes more frequent. Consequently, the wall pressure and the injection thrust are negligible unless the solar probe flies at smaller distance from the heliocenter than the nominal ($4Rs$).

2. Method of Numerical Simulation

To describe the three-dimensional complicated configuration of the solar probe (Fig. 1), we use the overset grid system shown in Fig. 5a. It consists of the background grid and four subgrids, each of which is generated around each part of the spacecraft body. Though the heat shield has circular or elliptic shape, orthogonal rectangular prism cells are used to keep the cell volume and shape uniform in each subgrid.

To simulate the rarefied flow of the solar wind and sublimation gas around the spacecraft, we use the DSMC method[12] with the modified Nanbu scheme.[16] In the DSMC method, the calculation at each time step is divided into two procedures, that is, update of the particle position by the translational motion and update of the molecular velocity by the collisions between particles. In the modified Nanbu scheme, the velocity of all of the test particles is updated once in each time step, after all of the collisions in the computational domain are calculated. Such an explicit procedure in the collision calculation is suitable for the overset grid system. To avoid double counting of the collision both in a subgrid and in the background grid, collisions of particles located in the overlapped region are calculated only once in a subgrid at each time stepping.

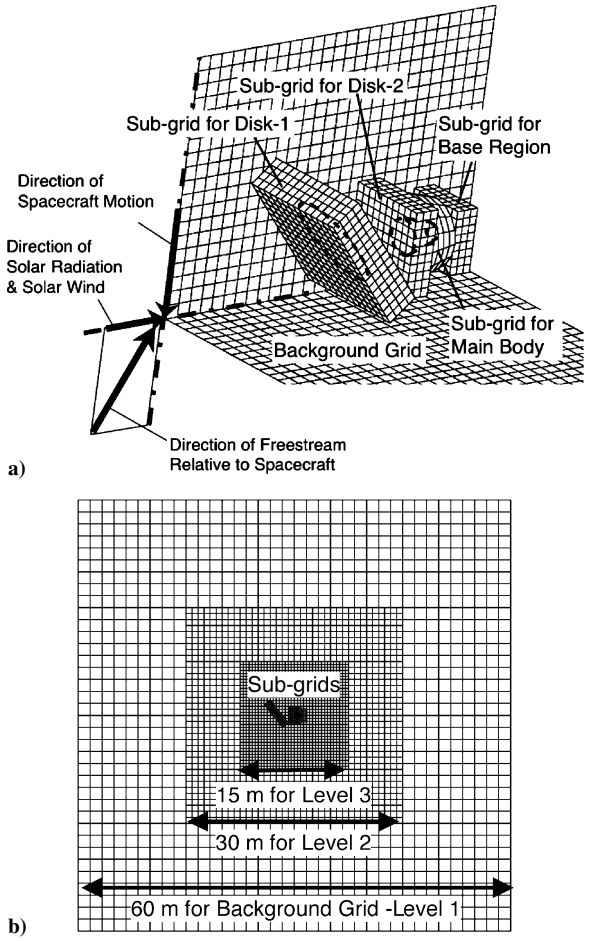

Fig. 5 Overset grid system around solar probe with inclined primary heat shield disk: a) subgrids in background grid and b) multilevel background grids for near-field analysis with solar wind.

Monatomic carbon is considered as the sublimation gas. When the sublimation rate is assumed, the sample particles for the sublimation gas are injected uniformly from the heat shield surface with the Maxwellian velocity distribution function at T_w. In the case with solar wind, we also consider monatomic hydrogen as the solar wind particles. The direction of the solar wind relative to the spacecraft is determined considering the attitude of the spacecraft and its trajectory is explained in Sec. IV.C and shown in Fig 5a. In the present study, the electromagnetic effects on the charged particles are not considered, although the dominant compositions of the solar wind are proton and electron. Chemical reactions including the electron impact ionization are also ignored. Consideration of these effects is left for future work. However, such a simplified model is expected to be capable of describing the essence of the phenomena, that is, the interaction between the solar wind and sublimation gas cloud though molecular collisions. For further simplification, the hard sphere model with the constant diameter of 3.4×10^{-10} m is used for both species. The effect of the molecular diameter is discussed in the far-field analysis. At the collision calculation, the difference in the particle mass between the solar wind and the sublimation gas is taken into account. The solar wind particles coming into the computational domain are given by the Maxwellian distribution function for the freestream condition. The sample particles going out of the computational domain are deleted from the calculation. For the gas–surface interaction, a diffusive wall is assumed for both species. Although there are a wide range of uncertainties in the gas–surface interaction model, their effects are expected to be negligible on the observation of the energetic particles in the solar wind because the velocity of the reflected particle is much lower than the freestream velocity and the molecular collision is not significant even in the vicinity of the surface in the present cases. In the case that only the sublimation gas is considered, the time step size is determined to be 40% of the mean collision time. In the case with the solar wind, the timescale for translation motion is much smaller than that for the collision because of extremely high velocity of incoming solar wind particles. The time step size is determined by setting the Courant number for the mean freestream velocity as 0.5. For the case without the solar wind, the size of the computational domain and the number of the computational cells are $20 \times 20 \times 20$ m^3 and $50 \times 50 \times 50$, respectively. The total number of the sample particles in the computational domain is about 600,000. For the case with the solar wind, the size of the computational domain is $60 \times 60 \times 60$ m^3, which is sufficiently larger than the length scale of the interaction between the solar wind and the sublimation gas. When the uniform grid is used, it is difficult to have a sufficient number of test particles in each cell of the background grid especially in the far field because the number density of the solar wind and the sublimation gas rapidly decreases with the distance from the spacecraft. To overcome this problem, the background grid is divided into three levels as shown in Fig. 5b. At each level, the computational domain is uniformly divided into $36 \times 36 \times 36$ cells. The total number of the sample particles in the computational domain is about 900,000.

To assess the credibility of the present overset grid method, we have solved a test problem beforehand. As the test problem, the rarefied flow around a circular disk with the sublimation gas injection in the solar wind is solved. The radius of the disk is 1.5 m. The freestream condition, the wall condition, the cell size, and the number of the test particles are the same as those in the near-field analysis with the solar wind except the body shape. For this configuration, the flow can be solved by either the single (equal to the nonoverset) grid or the overset grids. In the single-grid case, the Cartesian grid is used. The disk is set normal to the x axis and the solar wind comes in the x direction. In the overset grid case, the subgrid generated around the disk is put in the background Cartesian grid at 45 deg inclined to the x axis. The direction of the freestream is also inclined at 45 deg to the x axis. If the solution by the present overset grid method is correct, its solution will coincide with that of the single grid by rotating the coordinates by 45 deg because both the single-grid case and the overset-grid case essentially describe the same flow. We compare the density distribution of the solar wind along the centerline of the disk and evaluate their agreement by the integrated-and-normalized density difference, which is defined as

$$\frac{\int |n_{\text{single}} - n_{\text{overset}}| \, \mathrm{d}x_C}{\int n_{\text{single}} \, \mathrm{d}x_C}$$

where x_C denotes the coordinate along the centerline. The integration is numerically calculated by the linear interpolation method. When the size of the subgrid cells around the body is 0.25 m, the integrated-and-normalized density difference is 0.031. When the statistical error inevitable to the DSMC method is considered, this value is sufficiently small and it is confirmed that the present overset grid method works well for the rarefied flow conditions considered in the present study.

To check the convergence of the solution, the effect of the cell size is investigated. The effects of the number of time steps for data sampling and the number of test particles are discussed in the far-field analysis in Sec. IV.B. The same flowfield as in the credibility check is solved by the overset grid method varying the cell size of the subgrid from 1.0 to 0.2 m. The grid convergence is evaluated by the integrated-and-normalized density difference, which is defined as

$$\frac{\int |n - n_{0.2}| \, \mathrm{d}x_C}{\int n_{0.2} \, \mathrm{d}x_C}$$

where subscript 0.2 denotes the solution by using the finest grid. The integrated-and-normalized difference decreases with the cell size, and it becomes 0.04 for the cell size of 0.25 m. For the near-field analysis around the solar probe, the cell size of the subgrids is determined to be 0.25 m.

B. Far-Field Analysis

1. Length Scale Consideration

In the far-field analysis, the interaction between the solar wind particles and the sublimation gas particles is considered. At present, the properties of the solar wind in the corona are not well understood. However, according to the semiempirical model of the environment in the solar corona,[17] the mean velocity V_∞ and temperature T_∞ are around 100 km/s and 10^6 K, respectively. The number density n_∞ is expected to be in the range between 10^{12} and 10^{14} m^{-3}. To consider a severe case with respect to the interaction between the solar wind and the sublimation gas cloud, we assume 10^{14} m^{-3} as the number density in the corona because higher coronal density results in more significant interaction as explained later. Hence, the mean velocity, the temperature, and the number density are set as 100 km/s, 10^6 K, and 10^{14} m^{-3}, respectively, for the nominal freestream condition of the solar wind in the corona. In the present study, we assume that the solar wind is in the same direction as the solar radiation, although the direction of the solar wind does not coincide with that of the solar radiation due to the effect of the sun's rotation.

To begin with, the length scale of the phenomena must be determined. The sublimation gas injected from the heat shield spreads around the spacecraft and forms a cloud. When the size of the cloud and the number density in it are large, the solar wind particles will collide with the sublimation gas particles many times before they have passed through the cloud. Although the solar wind is a plasma, the neutral monatomic hydrogen is assumed as the component of the solar wind. The effects of charged particles and the presence of the electrons are ignored. Monatomic carbon is considered as the sublimation gas in the same way as in the near-field analysis. For simplicity of formulation, the hard sphere model is used for both the sublimation gas and the solar wind particles. The diameter of the solar wind particle is assumed to be the same as that of the sublimation gas (3.4×10^{-10} m), although the molecular diameter of monatomic hydrogen is 2.7×10^{-10} m in Ref. 13. The effect of the use of the equal cross section diameter is discussed later.

We consider that the sublimation gas is injected at the rate J_{sub} from the area S as shown in Fig. 6. Also, we assume that the sublimation gas is free molecular because the mean free path is larger than the spacecraft size in the nominal case as shown in Fig. 3. We consider the balance of mass flux between the sublimation gas injection and the outflow through a hemisphere with radius r (Fig. 6). When the radius is much larger than the size of the heat shield, it can be taken as a point source of gas injection. The number density at radius r and zenith angle ϕ is proportional to $\cos\phi$ and inversely proportional to the square of r. Consequently, the number density is obtained as

$$n = \frac{J_{\text{sub}} S \cos\phi}{m_p \pi r^2 C_{\text{av}}} \tag{5}$$

where C_{av} is the average molecular speed[14] of the gas in equilibrium at temperature T_w,

$$C_{\text{av}} = \sqrt{8(R/M_C)T_w/\pi} \tag{6}$$

In the far-field analysis, we assume that the heat shield is set normal to the solar direction. The results of the far-field analysis are not sensitive to the angle of the heat shield to the solar wind because the sublimation gas forms a cloud enveloping the spacecraft. The length scale L is defined as the distance between the source of gas injection and the point at which the number density of the sublimation gas is equal to that of the solar wind on the centerline, $\phi = 0$. The length scale L is calculated by setting $\phi = 0$ and $n = n_\infty$ in Eq. (5) as

$$L = \sqrt{\frac{J_{\text{total}}}{8\pi n_\infty m_p}} \sqrt{\frac{2\pi}{(R/M_C)T_w}} \tag{7}$$

where n_∞ and J_{total} are the number density of the solar wind and the total sublimation rate, respectively. When it is considered that the sublimation gas is injected to both sides of the heat shield, the total sublimation rate is evaluated as $2 J_{\text{sub}} S$. The mean free path is defined as the product of the mean collision time and the average traveling speed of the molecule. To make a more severe evaluation with respect to the collision effect, we should choose the formulation to give a smaller value for the mean free path. When the collision between the high-speed rarefied gas (solar wind) and low-speed dense gas (sublimation gas cloud) are considered, the mean collision time and the average traveling speed are calculated based on the velocity of a quickly moving particle (solar wind) and on the velocity of a slowly moving particle (sublimation gas), respectively. When the reference velocities for the solar wind particle and the sublimation gas are evaluated as the mean velocity V_∞ and the most probable molecular speed[14] C_{mp}, respectively, the mean free path for the interaction between the solar wind and the sublimation gas cloud is obtained as

$$\lambda = 1 \Big/ \left(\pi d^2 V_\infty n_\infty\right) \times C_{\text{mp}}, \qquad C_{\text{mp}} = \sqrt{2(R/M_C)T_w} \tag{8}$$

The Knudsen number referred to the length scale L in Eq. (7) is given by

$$Kn = \frac{\lambda}{L} = \frac{\sqrt{2(R/M_C)T_w}}{\pi d^2 V_\infty n_\infty L} = \frac{2^{\frac{7}{4}}}{\pi^{\frac{3}{4}}} \frac{1}{d^2 V_\infty} \left(\frac{R}{M_C} T_w\right)^{\frac{3}{4}} \sqrt{\frac{m_p}{n_\infty J_{\text{total}}}} \tag{9}$$

As seen in Eqs. (7) and (9), the length scale and the Knudsen number depend on the wall temperature of the heat shield, the number density of the solar wind, and the total sublimation rate. The Knudsen number also depends on the mean velocity of the solar wind. Figure 7 shows the variations of the length scale and the Knudsen number with the total sublimation rate for various freestream conditions of the solar wind. The wall temperature is set as 2500 K. The effect of the wall temperature is much smaller than the other factors. The number density of 10^{14} m^{-3} corresponds to the nominal coronal condition, and 10^{16} m^{-3} corresponds to an unexpectedly high-density condition, for example, the case of solar flare. Though the nominal solar wind velocity in the corona is considered as

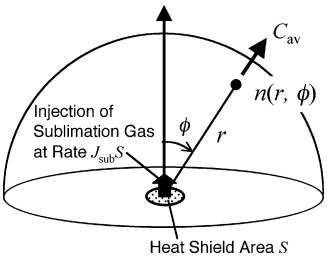

Fig. 6 Schematic of sublimation gas injection model.

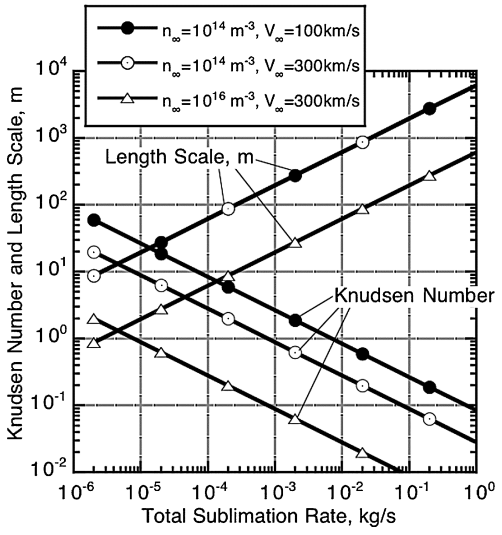

Fig. 7 Variation of length scale and Knudsen number with total sublimation rate for interaction between solar wind and sublimation gas cloud.

100 km/s, the speed of the incoming solar wind relative to the spacecraft motion becomes much higher because the flyby speed of the solar probe at the perihelion is planned to be about 300 km/s according to the trajectory analysis.[7] Equation (9) tells us that high flyby speed of the solar probe results in more severe interaction between the solar wind and the sublimation gas cloud because the Knudsen number decreases with the increase in the solar wind velocity. When the total sublimation rate increases, the Knudsen number decreases and the interaction becomes more significant. The length scale increases with the total sublimation rate. In some cases, the length scale is much larger than the spacecraft size. The increase in the number density of the solar wind also results in more significant interaction with smaller Knudsen number. However, the length scale of interaction decreases with the increase in the freestream number density.

The Knudsen number is inversely proportional to the cross section, and the evaluation of the cross section shows the first-order effect on the magnitude of the interaction between the solar wind and the sublimation gas. In the present study, we use the constant and equal cross section diameter. The present assumption is expected to result in an overprediction with respect to the collision effect between the solar wind and the sublimation gas for two reasons: 1) The molecular diameter of monatomic hydrogen is smaller than that of monatomic carbon. 2) The effective cross section of real molecules decreases as the relative speed of the colliding molecules increases.[12]

With regard to the first point, the molecular diameter of monatomic hydrogen is 2.7×10^{-10} m in Ref. 13. In the hard sphere model, the effective cross section diameter is obtained by averaging the cross section diameters of colliding molecules. For collision between monatomic hydrogen and monatomic carbon, the effective cross section diameter is 3.05×10^{-10} m and the Knudsen number becomes 1.24 times larger than that for the equal cross section diameter. The assumption of the equal cross section diameter yields a smaller Knudsen number and more significant collision effect. From Eq. (9), the use of the equal cross section diameter is equivalent to the consideration of larger total sublimation rate by a factor of 1.54. In other words, the use of the equal cross section diameter corresponds to the consideration of the safety margin of 54% in the total sublimation rate.

The use of the constant cross section diameter results in considerably severe limitation for the total sublimation rate. When the variable hard sphere (VHS) model is used with regard to the second point, the effective molecular diameter is given by[12]

$$d_{\mathrm{VHS}} = d_{\mathrm{ref}}\left[(c_{\mathrm{ref}}/c_r)^{\omega-\frac{1}{2}} \Big/ \sqrt{\Gamma\left(\tfrac{5}{2}-\omega\right)}\right], \qquad c_{\mathrm{ref}} = \sqrt{2kT_{\mathrm{ref}}/m_r} \tag{10}$$

where m_r and c_r are the reduced mass and the relative speed, respectively. Γ is the gamma function. The reference temperature T_{ref} is 273 K. The temperature exponent of the viscosity ω is calculated as 0.92 and 0.63 for monatomic hydrogen and monatomic carbon from the data in Refs. 18 and 10, respectively. This means that the effective cross section diameter for monatomic hydrogen decreases with the relative speed much more rapidly than that for monatomic carbon. For the collision between monatomic hydrogen and monatomic carbon, the relative speed is expected to be as high as the freestream velocity of the solar wind because the speed of the sublimation gas is negligible. For such high relative speed, the effective cross section diameter of monatomic hydrogen is much smaller than that of monatomic carbon. Consequently, the effective cross section diameter for the collision between monatomic carbon and monatomic hydrogen is smaller than the constant and equal cross section diameter by a factor of $0.5(c_{\mathrm{ref}}/V_\infty)^{0.13}$ ($c_{\mathrm{ref}} = 2.4$ km/s). This factor becomes 0.31 for $V_\infty = 100$ km/s. From Eq. (9), the use of the constant and equal cross section diameter is equivalent to the consideration of about 100 times larger total sublimation rate in the VHS model. Because the Knudsen number is inversely proportional to $d^2 V_\infty$ in Eq. (9), the Knudsen number is proportional to $V_\infty^{-0.74}$ for the VHS model. The trend that the Knudsen number decreases with the freestream velocity as seen in Fig. 7 is still observed even when the VHS model is used. However, the difference between the results of $V_\infty = 100$ and 300 km/s becomes smaller than the hard sphere model. When the wide range of uncertainties in the analysis model is considered, the assumption of the constant and equal cross section diameter makes the evaluation of the allowable total sublimation rate to be severe enough to meet various unexpected situations.

Figure 7 is very convenient for rough predictions about the extent of the interactions between the solar wind and the sublimation gas. We consider the interaction effect to be intolerably severe for solar wind observation, when the Knudsen number is smaller than unity. To determine the maximum allowable total sublimation rate with some safety margin, the freestream density of the solar wind is set as 10^{16} m^{-3}, considering the case of unexpectedly high density. From Fig. 7, the maximum allowable total sublimation rate is determined as about 10^{-5} kg/s.

2. *Method of Numerical Simulation*

To simulate the interaction between the solar wind and the sublimation gas, the DSMC method with the modified Nanbu scheme is also used in the same way as in the near-field analysis. In the far-field analysis, the solar probe is described as the point-source located at the center of the computational domain with the size $10L \times 10L \times 10L$ (L is the length scale of the phenomena given in Eq. (7)). The computational domain is uniformly divided into $40 \times 40 \times 40$ cells. The sample particles for the sublimation gas are injected at a specified total sublimation rate with the Maxwellian velocity distribution function from the point-source in both the solar direction and the opposite direction. The solar wind particles coming into the computational domain are given by the Maxwellian velocity distribution function for the freestream condition. The time step size is determined with the Courant number for the freestream velocity at 0.5, which corresponds to about 20–60% of the mean collision time. The total number of the test particles in the computational domain is about 500,000–700,000.

IV. Results and Discussion

A. Near-Field Analysis Without Solar Wind

Figure 8 shows the number density distribution of the sublimation gas around the solar probe on the plane of symmetry. In this case, the solar wind is not considered. The distance between the probe and the heliocenter is $4Rs$, and the radiative heating from the sun is 3.9 MW/m^2. The temperatures of disks 1 and 2 are calculated as 2279 and 1500 K, respectively. The wall temperature of the main body is assumed to be constant at 300 K. The total sublimation rate is 1.96×10^{-6} kg/s. The sublimation rate from disk 2 is negligible in comparison with that from disk 1. The thin dashed lines in Fig. 8 represent the interface lines between a subgrid and the background grid shown in Fig. 5a. The fact that the contour lines are smoothly drawn across the interface lines indicates that the present overset grid

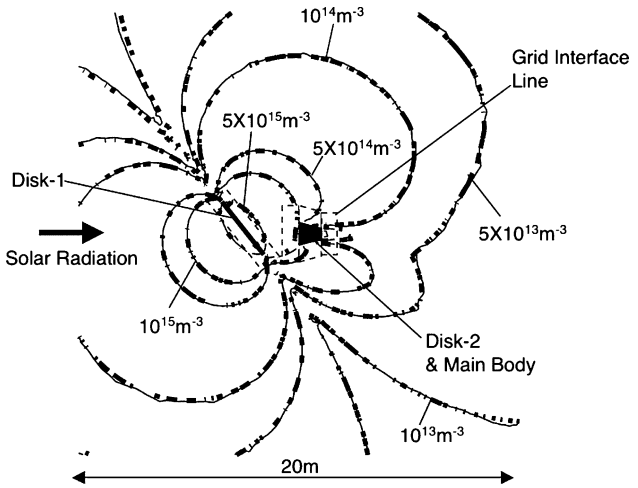

Fig. 8 Number density distribution of sublimation gas around solar probe on plane of symmetry: ——, DSMC results and - - - -, free molecular results.

system works successfully. It is clearly seen that the sublimation gas spreads smoothly from the heat shield to the ambient vacuum and forms a cloud around the solar probe. The maximum number density is obtained in the vicinity of the wall of disk 1 as 7.3×10^{15} m^{-3}, which is almost 100 times larger than the number density of the solar wind in the nominal coronal condition. The Knudsen number based on the maximum number density and the major diameter of disk 1, 3 m, is calculated as 85 by Eq. (4). Consequently, the flow of the sublimation gas around the spacecraft is considered to be free molecular. The amount of the sublimation gas reaching the base region behind the main body is quite small. To avoid the measurement noise due to the sublimation gas particles, the sensors should be located in the base region behind the main body.

The number density distribution of the sublimation gas can be predicted more easily under the assumption of free-molecular flow. When Eq. (5) is rewritten in integral form, the number density at an arbitrary point with radius r and zenith angle ϕ (Fig. 6) is calculated as

$$n = \int_{\text{field of vision}} \frac{J_{\text{sub}} \cos\phi}{m_p \pi r^2} \sqrt{\frac{\pi}{8(R/M_C)T_w}}\, \mathrm{d}S \qquad (11)$$

where the integral is made over the whole surface of the heat shield in the field of vision from the point. The result of this method is also plotted by thick dashed lines in Fig. 8. The result by the DSMC analysis agrees quite well with the result by using Eq. (11) because the flow of the sublimation gas is almost free molecular, as already discussed.

B. Far-Field Analysis

Figure 9 shows the number density distribution of the solar wind particles on the plane of symmetry at freestream velocity 100 and 300 km/s. The freestream temperature and the number density of the solar wind are 10^6 K and 10^{14} m^{-3}, respectively. To clarify the characteristic features of the interaction phenomena between the solar wind and the sublimation gas cloud, the total sublimation rate is set as 2×10^{-2} kg/s, which is much higher than the allowable level. The sublimation gas is injected in both the solar direction and the opposite direction with the Maxwellian distribution at temperature 3000 K. When the pattern of the number density distribution is considered, the length scale of the phenomena is estimated as about 1 km for both cases. This length scale is almost the same as predicted from Fig. 7. In the case of 100 km/s, the number density of the solar

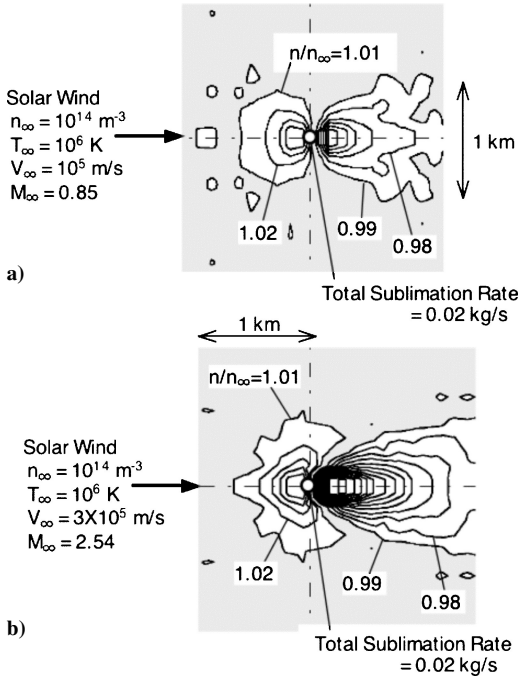

Fig. 9 Number density distribution of solar wind particles at freestream velocity a) 100 km/s and b) 300 km/s.

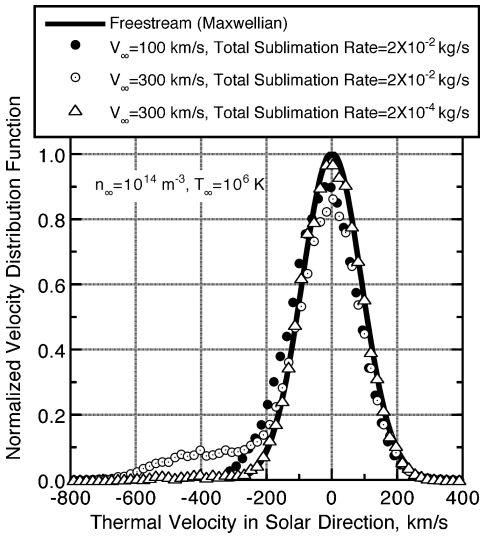

Fig. 10 Effect of freestream velocity and total sublimation rate on velocity distribution function observed at solar probe.

wind increases by about 5% in front of the probe due to the collision with the sublimation gas cloud. In the wake region behind the solar probe, the number density decreases by 7–8%. Such flow features are also observed in the case of 300 km/s. However, the density decrease in the wake region becomes more significant than in the case of 100 km/s.

The velocity distribution function of the solar wind is one of the most important measuring items for understanding the mechanism of the coronal acceleration and heating. The velocity distribution function of the solar wind particles is calculated at the probe location, for various conditions. Sampling of the test particles is made in a $0.5L$ cube around it. In the present study, the distribution function with respect to only the velocity component in the solar direction is considered. Figure 10 shows the effects of the total sublimation rate and the freestream velocity on the velocity distribution function. The distribution function is normalized by the peak value of the distribution function in the freestream. The horizontal axis is the thermal velocity, which is defined as the difference from the mean velocity. The number of particles at lower velocity increases and that at higher velocity decreases in comparison with the distribution function of the freestream. This fact indicates that the solar wind is decelerated by the molecular collision with the sublimation gas cloud. The properties of the solar wind observed at the probe become different from those of the undisturbed freestream due to the presence of the sublimation gas cloud. To obtain almost the same distribution as the undisturbed freestream at the probe, the total sublimation rate must be reduced to 2×10^{-4} kg/s. In the case of the freestream velocity 300 km/s and the total sublimation rate 2×10^{-2} kg/s, a plateau is clearly seen in the left foot of the distribution function. The plateau is still observed even when the total sublimation rate is 2×10^{-4} kg/s. Such a pattern is observed only in the case of supersonic inflow. It disappears when the flow is subsonic at Mach number 0.85 for the case of 100 km/s.

The accuracy of the solution by the DSMC method depends on the number of time steps for data sampling, the number of the test particles, and the cell size. In the present study, these parameters are determined after a series of test calculations. As a test problem, the solar wind flow shown in Fig. 9b is selected. The freestream velocity, density, temperature, and total sublimation rate are 300 km/s, 10^{14} m^{-3}, 10^6 K, and 0.02 kg/s, respectively. We compare the integrated-and-normalized difference in the velocity distribution function of the solar wind at the probe location for various computational parameters. The integrated-and-normalized difference, which is defined as

$$\frac{\int |f - f_{\text{ref}}|\, \mathrm{d}c}{\int f_{\text{ref}}\, \mathrm{d}c}$$

(where f_{ref} and c are the result shown in Fig. 10 and the molecular velocity, respectively) becomes smaller than 0.02 when the number

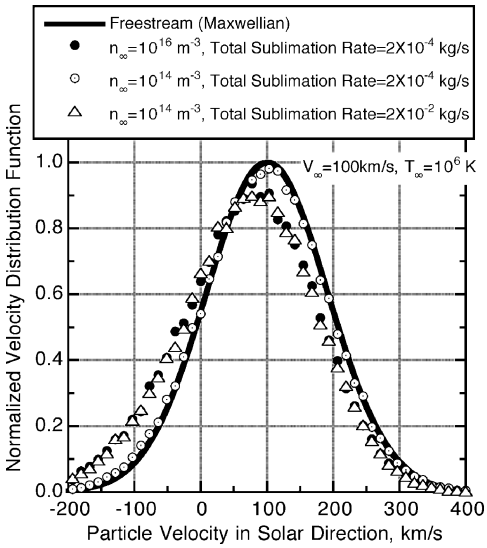

Fig. 11 Effect of freestream number density and total sublimation rate on velocity distribution function observed at solar probe with freestream velocity 100 km/s.

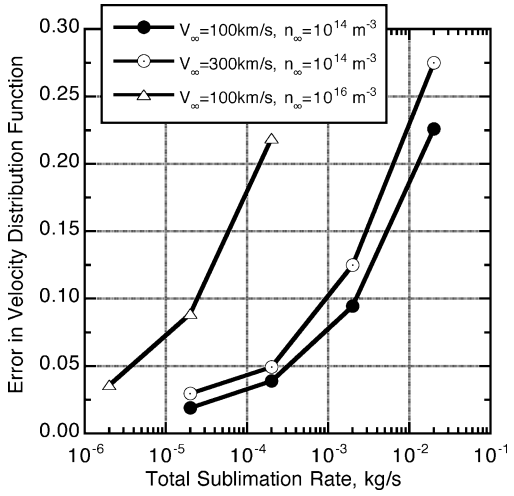

Fig. 12 Variation of observation error in velocity distribution function of solar wind with total sublimation rate.

of time steps for data sampling becomes larger than 5000. As for the number of the test particles, we found that the averaged particle number per cell must be larger than 3 for the integrated-and-normalized difference to be smaller than 0.03. When the cell size becomes smaller than $0.3L$, the integrated-and-normalized difference becomes smaller than 0.03. Further reduction in the integrated-and-normalized difference is not obtained by increasing the number of time steps, the number of test particles, or decreasing the cell size because of a statistical error in the DSMC method. In the far-field analysis, the computational parameters are set to satisfy the preceding convergence criteria.

Figure 11 shows the effect of the freestream number density of the solar wind and the total sublimation rate on the velocity distribution function. The freestream velocity is 100 km/s. The distribution function at the total sublimation rate 10^{-4} kg/s and the number density of the solar wind 10^{16} m^{-3} is similar to that at 10^{-2} kg/s and 10^{14} m^{-3}. With regard to the interaction between the solar wind and the sublimation gas cloud, the increase in the freestream number density causes the same effect as the increase in the total sublimation rate. This fact is already predicted in Eq. (9), where the Knudsen number depends on the product of n_∞ and J_{total}. When it is considered that there is a large uncertainty in the number density of the solar wind in the corona, it is recommended that the maximum allowable value for the total sublimation rate should be in the order of 10^{-6} kg/s or lower for the sensors to still work in unexpectedly high-density corona such as 10^{16} m^{-3}.

We evaluate the difference in the velocity distribution function of the solar wind from the undisturbed freestream by the observation error defined as

$$\text{observation error} = \frac{\int |f - f_\infty| \, \mathrm{d}c}{\int f_\infty \, \mathrm{d}c} \tag{12}$$

where f_∞ is the Maxwellian distribution function in the freestream and the integral is made over the whole velocity space. The variation of the observation error with the total sublimation rate is shown in Fig. 12 for various freestream conditions. The observation error mainly depends on the total sublimation rate and the coronal density. The error also increases with the increase in the freestream velocity, but its effect is not so large as that of the other factors. From Fig. 12, the total sublimation rate should be smaller than 2×10^{-6} kg/s for the observation error to be smaller than 5% even in the case of high density corona at 10^{16} m^{-3}.

C. Near-Field Analysis in the Presence of Solar Wind

To find an appropriate location for the sensors, the near-field analysis is made in the presence of the solar wind. Figure 13 shows the

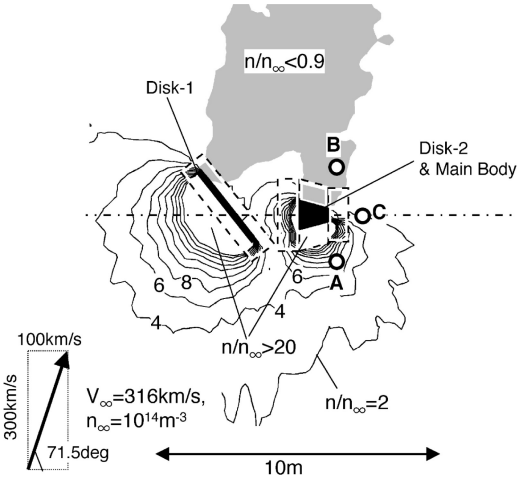

Fig. 13 Number density distribution of solar wind particles around solar probe.

number density contours of the solar wind on the plane of symmetry. The spacecraft shape, the distance from the heliocenter, and the total sublimation rate are the same as in the case shown in Fig. 8. The spacecraft is shown to be moving from the top to the bottom of Fig. 13: At 300 km/s, disk 1 collides with the solar wind at velocity of 316 km/s, and the incidence, which is the angle between the freestream vector and the normal vector of disk 1, is 33 deg. Such high incidence is caused by the high flyby speed and the spacecraft attitude pointing to the sun. The freestream number density and temperature are set as 10^{14} m^{-3} and 10^6 K, respectively. In this case, the near-field analysis can detect the interaction phenomena between the solar wind and the sublimation gas cloud because the length scale for the interaction is estimated as about 10 m from Fig. 7. Two types of phenomena are expected in the result, that is, the interaction between the solar wind and the sublimation gas cloud and the gas–surface interaction for the incoming solar wind particles. However, the former is not remarkable because the total sublimation rate is lower than the allowable level. In the windward side of both disk 1 and the main body, regions of very high density appear. Such regions are not observed in the far-field analysis. They are formed by reemission of the slowly moving particles reflected at the surface of the body. In the leeward region, the number density decreases and the wake is formed behind the spacecraft.

Figure 14 shows the velocity distribution function in the solar direction at points A–C indicated in Fig. 13. Sampling of the test particles is made in a 0.83-m cube around each point. Both the solar wind particles and the sublimation gas particles are taken into account in the distribution function. The sublimation gas particles

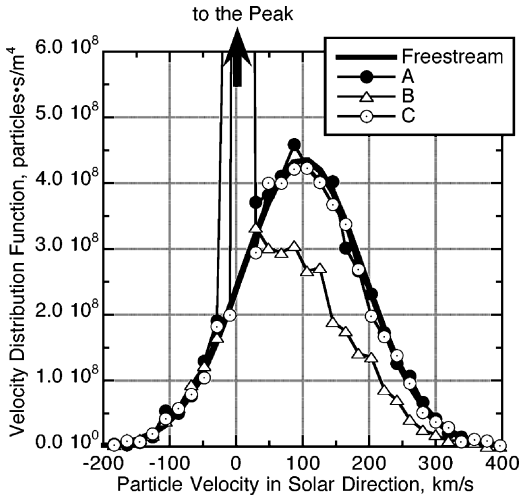

Fig. 14 Effect of measurement location on velocity distribution function.

are quite slow in comparison with the solar wind particles and are observed only in the velocity region from −50 to +50 km/s. In the other velocity regions, the solar wind particles are only observed. At all of the observation points, a steep peak is seen in the velocity region around 0 km/s. This peak is formed from the sublimation gas particles and the slowly moving solar wind particles reflected at the diffusive wall of the spacecraft. At points A and C, the obtained distribution function is almost the same as that of the freestream, except this peak. For particle velocity higher than 50 km/s, no significant discrepancy from the freestream condition is observed. This fact indicates that the presence of the high-density regions in the windward side of the spacecraft does not affect significantly the measurement of the energetic particles in the solar wind. However, at point B, which is located in the wake as shown in Fig. 13, the distribution function is much different from that of the freestream because some amount of the solar wind particles cannot reach point B due to the presence of the spacecraft body in front of it. Points A and B correspond to the case where the sensors for the solar wind observation are put at the top of the boom and extended sideways from the base of the main body. Point C corresponds to the case of a boom extended on the centerline. In the former case, careful control of the roll angle is always necessary during the solar flyby for the sensors not to be in the wake of the spacecraft. Consequently, the sensors for the solar wind observation should be put on the top of the boom extended from the base of the spacecraft on the centerline as shown in Fig. 1. For reduction in the observation error caused by the presence of the sublimation gas particles and the solar wind particles reflected at the wall, the boom length should be large enough under the constraint that the boom and the sensors must be in the shade of the heat shield. In the present case, the boom length of 1 m, which corresponds to point C, is appropriate.

V. Conclusions

The major conclusions of the present study are as follows:

1) The multiple-stage graphitic disks with the most forward primary disk inclined to the solar direction are promising for the heat shield configuration of the solar probe from the viewpoint of reduction in the shield mass and total sublimation rate.

2) The method to evaluate the length scale and the Knudsen number for the interaction phenomena between the solar wind and the cloud of the sublimation gas is proposed. The increase in the sublimation rate results in smaller Knudsen number and more significant interaction. The increase in the freestream number density of the solar wind also produces a similar result. When the sublimation rate is large, the interaction occurs at length scales larger than the size of the spacecraft.

3) The properties of the solar wind observed by the solar probe in the corona may be disturbed due to the molecular collision with the sublimation gas cloud injected from the probe itself. The DSMC analyses assuming a point source of sublimation gas injection in the solar wind show that the velocity distribution function of the solar wind obtained by the solar probe may be different from that of the undisturbed freestream. The difference becomes significant when the total sublimation rate of the heat shield and the freestream number density of the solar wind are large. Consequently, the maximum allowable value for the total sublimation rate is about 2×10^{-6} kg/s.

4) To find an appropriate place for the sensors of the solar wind, the rarefied flow of the solar wind and the sublimation gas around the solar probe is numerically analyzed by the DSMC method. The spacecraft configuration consisting of the heat shield and the main body is described by the overset grid technique. For reduction in the observation error due to the presence of the sublimation gas particles and the slowly moving solar wind particles reflected at the surface, the sensors for the solar wind observation should be put on top of the boom extended from the base of the spacecraft along the centerline.

Acknowledgment

This work is supported in part by Grant-in-Aid for Scientific Research 17360408 of the Japan Society for the Promotion of Science.

References

[1]Millard, J. M., Maag, C. R., and Miyake, R. N., "STARPROBE Thermal Shield System Design Concept," *Entry Vehicle Heating and Thermal Protection Systems*, edited by P. E. Bauer and H. E. Collicott, Vol. 85, Progress in Astronautics and Aeronautics, AIAA, New York, 1983, pp. 351–384.

[2]Park, C., "Preliminary Design Study of Solar Probe Heat Shields," *Spacecraft Radiative Transfer and Temperature Control*, edited by T. E. Horton, Vol. 83, Progress in Astronautics and Aeronautics, AIAA, New York, 1982, pp. 439–471.

[3]Lundell, J. H., "Graphitic Heat Shield for Solar Probe Missions," *Spacecraft Radiative Transfer and Temperature Control*, edited by T. E. Horton, Vol. 83, Progress in Astronautics and Aeronautics, AIAA, New York, 1982, pp. 472–500.

[4]Kerridge, S., Evans, M., and Tsurutani, B., "Cost-Effective Mission Design for a Small Solar Probe," *Acta Astronautica*, Vol. 35, Suppl., 1995, pp. 257–266.

[5]Preble, J. C., and Tribble, A. C., "Small Solar Probe," *Journal of Spacecraft and Rockets*, Vol. 33, No. 5, 1996, pp. 729–733.

[6]McNutt, R. L., Jr., Krimigis, S. M., Cheng, A. F., Gold, R. E., Farquhar, R. W., Roelof, E. C., Coughlin, T. B., Santo, A., Bokulic, R. S., Reynolds, E. L., Williams, B. D., and Willey, C. E., "Mission to the Sun: The Solar Pioneer," *Acta Astronautica*, Vol. 35, Suppl., 1995, pp. 247–255.

[7]Guo, Y., and Farquhar, R. W., "Current Mission Design of the Solar Probe Mission," *Acta Astronautica*, Vol. 55, No. 3–9, 2004, pp. 211–219.

[8]Rohsenow, W. M., Hartnett, J. P., and Young, I. C. (ed.), *Handbook of Heat Transfer*, 3rd ed., McGraw–Hill, New York, 1998, Chap. 7.

[9]Randolph, J., Ayon, J., Dirling, R., Imbriale, W., Miyake, R., Le Queau, D., Olalde, G., Pierson, E., Rawal, S., Rivoire, B., Robert, J. F., Royere, C., Taylor, R., Valentine, P., and Vaughn, W., "The Solar Probe Shield/Antenna Materials Characterization," *Carbon*, Vol. 37, No. 11, 1999, pp. 1731–1739.

[10]Blottner, F. G., "Prediction of Electron Density in the Boundary Layer on Entry Vehicles with Ablation," *The Entry Plasma Sheath and Its Effects on Space Vehicle Electromagnetic Systems*, Vol. 1, NASA SP-252, 1970, pp. 219–240.

[11]Baker, R. L., "Graphite Sublimation Chemistry Nonequilibrium Effects," *AIAA Journal*, Vol. 15, No. 10, 1977, pp. 1391–1397.

[12]Bird, G. A., *Molecular Gas Dynamics and the Direct Simulation of Gas Flows*, Oxford Univ. Press, New York, 1994, Chaps. 2 and 9.

[13]Svehla, R. A., "Estimated Viscosities and Thermal Conductivities of Gases at High Temperatures," NASA TR R-132, 1962.

[14]Vincenti, W. G., and Kruger, C. H., Jr., *Introduction to Physical Gas Dynamics*, Wiley, New York, 1965, Chaps. 1 and 2.

[15]Suzuki, K., "Numerical Study on Behavior of Outgas from Heat Shield of Solar Probe," AIAA Paper 2004-2271, June–July 2004.

[16]Nanbu, K., "Stochastic Solution Method of the Boltzmann Equation II. Simple Gas, Gas Mixture, Diatomic Gas, Reactive Gas, and Plasma," Vol. 8, Inst. of Fluid Science, Tohoku Univ., Sendai, Japan, 1996, pp. 77–125.

[17]Sittler, E. C., Jr., and Guhathakurta, M., "Semiempirical Two-dimensional Magnetohydrodynamic Model of the Solar Corona and Interplanetary Medium," *Astrophysical Journal*, Vol. 523, No. 2, 1999, pp. 812–826.

[18]Zoby, E. V., Graves, R. A., Jr., Moss, J. N., Kumar, A., and Simmonds, A., "Transport Property Correlations for H–He Gas Mixtures at Temperatures of 1000–25,000K," *AIAA Journal*, Vol. 18, No. 4, 1980, pp. 463–470.

I. Boyd
Associate Editor